INTERNATIONAL JOURNAL OF AUTOMOTIVE AND MECHANICAL ENGINEERING
ISSN: 2229-8649 e-ISSN: 2180-1606
VOL. 21, ISSUE 3, 2024, 11629 – 11640
DOI: https://doi.org/10.15282/ijame.21.3.2024.14.0897

RESEARCH ARTICLE

Reconstructing Magnetic Hysteresis Behavior with Flux Model and Identifying Parameters for Dual-Coil MR Actuator

L. Tang[1,2*], W. Bankosz[1], J. Goldasz[1]

[1]Faculty of Electrical and Computer Engineering, Cracow University of Technology, Warszawska 24, 31-155 Krakow, Poland
[2]Department of Electrical Engineering, Electronics and Automatic Control, University of Girona, 17071 Girona, Spain

ABSTRACT - Magnetorheological (MR) actuators represent an important class of semi-active devices that have received extensive investigation and deployment in the field of vibration reduction systems. Their notable features include a significant reduction in energy consumption, along with an impressive tunable range of continuously controllable damping forces. The force output of these devices is a complex function that involves two hysteretic mechanisms: magnetic and mechanical (i.e. hydraulic). While the total hysteresis mechanism of these devices has been the subject of considerable study, comparatively little attention has been paid to their magnetic hysteretic behavior. In this study, the authors examine the behavior of the dual coil MR actuator's control circuit and attempt to extract the magnetic flux information from the laboratory measurements of electrical signals applied to it. The study is further enhanced by the incorporation of the Bouc-Wen (B-W) hysteretic unit, which serves to replicate the flux-current (or magnetic) hysteretic relationship. The B-W model's parameters are identified through the use of a hybrid algorithm, namely the particle swarm optimization and fmincon hybrid optimizing strategy. It incorporates the advantages of both algorithms, resulting in an average improvement of 0.38% in standard deviation compared to fmincon, across 1A to 5A, when comparing the experimental and simulation data. This strategy is employed to fit the model predictions to the flux data, derived from the reconstructed flux and current in time histories. The findings of the study demonstrate that the B-W model is an effective tool for predicting the variation in magnetic flux in response to an exciting current. The results can be implemented for prototyping or validating a model-based controller for MR actuator systems.

ARTICLE HISTORY
Received : 29th May 2024
Revised : 14th Aug. 2024
Accepted : 01st Sept. 2024
Published : 20th Sept. 2024

KEYWORDS
MR actuators
Magnetic hysteresis
Flux hysteresis
Bouc-Wen model
Parameter identification
Hysteresis

1. INTRODUCTION

The magnetorheological (MR) damper demonstrates excellent performance in both vehicle handling stability and driving comfort. As a result, many researchers have focused on MR dampers, leading to an in-depth exploration of their characteristics. Among these, the property of hysteresis has emerged as particularly significant. Consequently, numerous hysteretic models have been developed to capture this behavior in MR dampers. These models can generally be categorized into two types of hysteresis: mechanical and magnetic. From a mechanical hysteresis perspective, various parametric and non-parametric models have been proposed to accurately describe hysteresis behavior. Examples include the Bingham plastic model [1], bi-viscous modified Bingham model [2], Bouc-Wen model [3][4], large-scale dynamic model [5], polynomial models [6][7], and Sigmoid models [8][9]. These models are widely used for their ability to effectively predict the hysteretic behavior of output force in relation to velocity or piston displacement.

Additionally, from a magnetic perspective, it is important to consider various magnetic hysteresis models that have been developed, such as the Preisach hysteresis model, the J-A (Jiles-Atherton) model, the Duhem hysteresis model, and others. These models are well-established in the field of magnetic hysteresis estimation. Mayergoyz et al. (1989) developed the Preisach model, which experimental tests with two magnetic tape materials validated as more accurate for small reversal values and equally accurate for larger reversal values [10]. Seong et al. (2009) conducted an experimental test with an MR damper, predicting field-dependent hysteresis behavior using the Preisach model. They also combined a feedforward hysteretic compensator with the bi-viscous Bingham model to achieve the desired damping force [11]. In 1986, Jiles and Atherton [12] proposed a mathematical model for magnetic hysteresis that accounted for domain wall motion and pinning effects at defect sites, capturing key hysteresis features. Chua et al. (1970) [13] introduced the Duhem model, which demonstrated that hysteresis exhibited small loops that increased with frequency, revealing the hysteretic behavior of inductance. Macki et al. [14] discussed several hysteretic models, including the Duhem model, which used differential equations to represent hysteresis behavior, focusing on how the output changes when the input reverses direction. In 2020, Goldasz et al. [15][16] proposed a dual hysteresis concept, using the Duhem model to extract magnetic hysteretic behaviors and then analyzing it with Maxwell's first-order model. In 2019, Bai et al. [17] introduced an RC operator-based magnetic hysteresis model, highlighting the differences between electrical circuits and mechanical systems. Later, in 2020, Li [18] integrated the RC operator hysteresis model with a real-time control algorithm within a quarter-car model framework. Meanwhile, Bui et al. [19][20] developed the parametric Magic Formula hysteresis model, which demonstrated an enhanced ability to capture hysteresis behavior in MR dampers.

***CORRESPONDING AUTHOR | L. Tang** | ✉ u1955536@campus.udg.edu

However, the models mentioned above were derived from the relationship between flux density and field strength (B-H), which can be measured through testing. In this paper, we propose a new approach to identifying flux hysteresis by reconstructing one of the most effective and popular mechanical models, the Bouc-Wen model, and adapting it to account for electrical and magnetic effects. The Bouc-Wen flux hysteresis model aims to translate the behavior of mechanical hysteresis into the magnetic domain. To enhance the accuracy of parameter extraction, we design a PSO-fmincon hybrid method for parameter identification. Particle Swarm Optimization (PSO) is used in the initial stage due to its advantages in computational cost and performance over many soft computing algorithms [21]. Once the PSO finds optimal solutions, the fmincon algorithm is employed as a secondary optimizer to ensure the highest accuracy. This two-phase process guarantees that the final results surpass what either PSO or fmincon could achieve individually. With magnetic hysteresis accurately modeled, it would be possible to implement precise control of vehicle suspension by replacing the current command with a flux command. This approach could potentially reduce system delays caused by the conventional current command.

2. REVIEW OF THE CONVENTIONAL (MECHANICAL/HYDRAULIC) HYSTERESIS

Mechanical hysteresis has been extensively studied, particularly in relation to the force, piston displacement (i.e., suspension vertical travel), and piston velocity (i.e., vibration frequencies). This phenomenon occurs due to the reciprocating motion of the piston. Figure 1(a) presents a map of the damping force tested at a fixed current of 5A, with velocity varying from 0.1 m/s to 2.0 m/s in line with the piston stroke. From another perspective, as shown in Figure 1(b), the hysteresis was captured in the relationship between damping force and the peak velocity of the piston. The mechanical hysteresis illustrates energy absorption, and the data in Figure 1 indicate that the highest velocity produces the largest hysteresis loop. This suggests that at the specific current of 5A, the piston velocity of 2.0 m/s results in the greatest energy consumption.

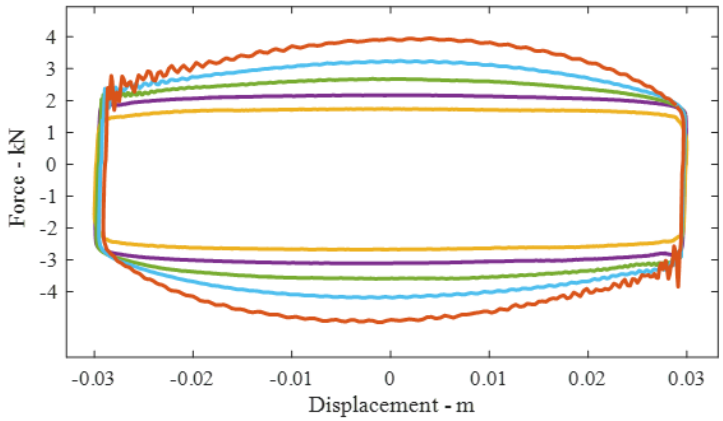

(a) Experimental damping force vs piston displacement

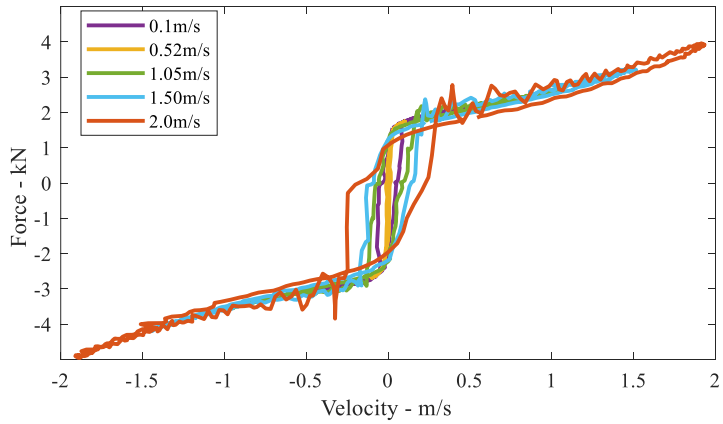

(b) Experimental damping force vs piston peak velocity

Figure 1. Hydraulic/Mechanical hysteresis, MR damper performed at 5A

Furthermore, in relation to mechanical hysteresis, an additional loop can be derived based on the velocity-displacement relationship, as shown in Figure 2. In this case, each loop corresponds to the peak velocity. While this relationship is generally considered less significant in practical applications compared to the force-velocity or force-displacement relationships, it still provides valuable insights into the mechanics of hysteresis in MR dampers.

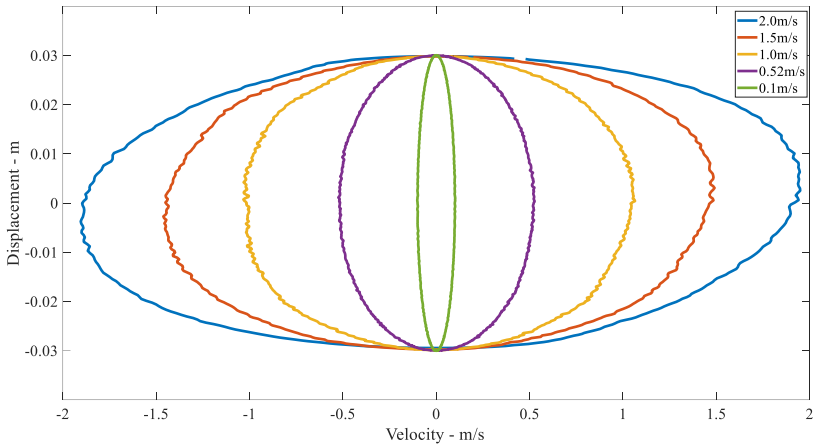

Figure 2. Hysteresis for velocity vs displacement, MR damper performed at 0A

To be precise, the mechanical hysteresis encompasses the magnetic hysteresis. However, this is not discernible in mechanical models, which is why the author wishes to present the magnetic hysteresis behavior. Consequently, the magnetic hysteresis will be extracted from the mechanical hysteresis in this article. The magnetic hysteresis can capture the voltage command with its frequency to describe the time delay in comparison to the output current gains.

3. CONSTRUCT THE MAGNETIC FLUX HYSTERETIC MODEL

As mentioned above, the conventional characteristics of hysteresis in MR damper generally combine hydraulic hysteresis and magnetic hysteresis. However, researchers mainly focused on hydraulic hysteresis because it is easier to be aware of it from experimental testing. Thus, the flux hysteretic concept is addressed to explain the hysteresis of MR damper from the magnetic perspective as well as explain how parameters affect the hysteretic shapes so that the hysteresis is understood as transferred from mechanical hysteresis to magnetic aspects. In this article, the flux was obtained by means of indirect measurements, where the inputs are voltages and the outputs are currents. To simplify equations, the flux will be replaced by flux linkage shown in the following equation (1).

$$\lambda = n \cdot \varphi \tag{1}$$

In the beginning, an output equation of the current i_c can be formulated as equation (2), where u is the input voltage and R_c is coil resistance.

$$i_c = \frac{1}{R_c}(u - \frac{d\lambda}{dt}) \tag{2}$$

However, λ is actually an unknown value that needs to be determined by means of measuring circuit current i_c, so that the equation can be operated from equation (2) to equation (3), where λ_0 is a reductant value by an integral operation, which means the initial linkage is an unknown value that needs to be estimated in the case of an indirect measuring method. However, it appears to be a known value in the case of direct measurement.

$$\lambda = \lambda_0 + \int (u - i_c R_c)\, dt \tag{3}$$

with an extra parameter – the coil inductance L_c, combine it with typical Bouc-Wen equations, shown in equation (4), the model can be reconstructed into the magnetic model or flux hysteretic model, shown below in equation (5).

$$\begin{cases} F = c\dot{x} + k(x - x_0) + \alpha z \\ \dot{z} = -\gamma \cdot |\dot{x}| \cdot z \cdot |z|^{n-1} - \beta \cdot \dot{x} \cdot |z|^n + \kappa \cdot \dot{x} \end{cases} \tag{4}$$

where in the formulations (4) and (5), the parameters $\alpha, \beta, \kappa, \gamma, k, D$, A are shape affecting values, z stands for hysteretic evolution variable, A was extracted from parameter α, but they have different tuning ranges and different perspective definitions. n_1, n_2 are shape sizing-related values, they can be uniform to be the same value in the case that the model has a good convergence, but it needs to be highlighted again that they are not the same parameter n in Bouc-Wen's.

$$\begin{cases} \lambda = \mathrm{A} \cdot L_c \cdot I_c + (1 - A) \cdot L_c \cdot D^{-1} \cdot z \\ \dfrac{dz}{dt} = \kappa \cdot \dfrac{di_c}{dt} - \beta \cdot \dfrac{di_c}{dt} \cdot |z|^{n_1} - z \cdot \gamma \cdot \left|\dfrac{di_c}{dt}\right| \cdot |z|^{n_2 - 1} \end{cases} \tag{5}$$

4. PARAMETER IDENTIFICATION PROCESS

A hybrid optimizing strategy was applied to identify the parameters. The authors would propose PSO (Particle Swarm Optimization) [22]-[24] to search for the best individuals while using fmincon for ending backup optimizing for the purpose of real best just in case PSO searching capability was not as good as fminicon. PSO keeps on working to search

for the minimum value as best, for individual best (P_best) and global best (G_best). The variables of the particle velocity and the searching position indicate the tuning efficiency of the optimization. They are important and should be considered in the iteration loop of programming [25] [26].

$$v_{t+1} = \omega_t v_t + c_1 r_1 (P_{best} - x_t) + c_2 r_2 (G_{best} - x_t) \tag{6}$$

$$x_{t+1} = v_{t+1} + x_t \tag{7}$$

In the above-mentioned equations (6) (7), v, x are for velocity and position, where the random parameters present as r_1, r_2, and t means the working iteration. And acceleration coefficients c_1, c_2 are shown in equations (8) (9), where c_{1_0}, c_{2_0}, and c_{1_end}, c_{2_end} are initial acceleration coefficients and finishing acceleration coefficients, respectively, and it means the number of total trials for iterations.

$$c_1 = \frac{t}{it}\left(c_{1\_0} - c_{1\_end}\right) + c_{1\_end} \tag{8}$$

$$c_2 = \frac{t}{it}\left(c_{2\_0} - c_{2\_end}\right) + c_{2\_end} \tag{9}$$

The ω, ω_{max}, and ω_{min} are consisting of a function for inertia weighting values shown as equation (10) indicates the optimizing capability for the PSO algorithm, where ω_{max} and ω_{min} are respectively the values for beginning and ending.

$$\omega = \omega_{max} - \frac{t}{it}(\omega_{max} - \omega_{min}) \tag{10}$$

To address the solutions in programming, the equations (6)-(10) should be defined with equations $v_t = v_{ij}(t)$, and $x_t = x_{ij}(t)$, for the sake of better programming codes, in which i, j, stand for i-th particle and j-dimensional searching space. The following pseudocode helps to understand the process of algorithms.

for i = 1 to n,

for j = 1 to m,

Do v_{ij} rand boundary,

Do x_{ij} rand boundary,

P_{best} = P_i at x_t,

G_{best} = $G_i \rightarrow min\ \{\ f(P_i)\ \}$,

While t≤max iteration,

for i = 1 to n,

for j = 1 to m,

Do equation (6),

Do equation (7)

Do $G_i \rightarrow min\ \{\ f(P_i)\ \}$,

t = t+1,

Do G_{best},

Start fmincon algorithm.

The fmincon is a constrained nonlinear program algorithm that solves the multivariable function to get the minimum solution. It is one of the most efficient and most utilized algorithms to deal with nonlinear parametrical models for obtaining proper parameters from estimation.

$$\min f(x)\ \ such\ that \begin{cases} c(x) \le 0 \\ ceq(x) = 0 \\ A \cdot x \le b \\ Aeq \cdot x = beq \\ lb \le x \le ub \end{cases} \tag{11}$$

In the above equation (11), $ceq(x)$ and $c(x)$ are limiting functions to perform the optimization, they are considered as a second boundary for both linear and nonlinear systems after the input lower boundary lb and upper boundary ub. Where the sub-equation, $A \cdot x \le b$ and $Aeq \cdot x = beq$ are the true targets for nonlinear systems that narrow the optimizing limitation. However, only nonlinear equations are utilized for the identifying process; hence, the equation can be simplified, as shown in equation (12), for a nonlinear system.

$$\min f(x) \ such \ that \ \{Problem_{min} \leq x \leq Problem_{max}\} \tag{12}$$

The experimental data of voltages and currents were sent into estimation. During the process, 1Hz, 5Hz and 10Hz frequencies of the voltages were employed to generate aptitude current from 1A to 5A. After the iteration is done, a cost function is used to check the errors between experimental data and the predicted values shown in equation (13).

$$\delta = \sqrt{\frac{1}{n}\sum_{i=1}^{n}(\lambda_{exp_i} - \lambda_{est_i})^2} \tag{13}$$

where the cost function is employing the concept of root mean squared error (RMSE), where λ_{exp_i} is the measured flux linkage and λ_{est_i} stands for estimated flux linkage.

5. RESULTS AND DISCUSSION

The approach to parameter identification using hybrid algorithms was discussed in the previous section, and the results and findings will be presented in this section. The feasibility of the proposed flux model and its application for parameter identification have been validated and aligned with experimental data analysis. In this study, the experimental data were obtained from tests conducted on a specific commercial MR damper with dual coils. Figure 3(a) illustrates the cross-section of the piston for the dual-coil damper, which distinguishes it from single-coil dampers. The dual coils can either generate more magnetic flux or reduce it, allowing for various control strategies.

Figure 3(b) shows a detailed diagram of the measurement system, where a computer acts as the master device, controlling the entire process. The computer sets the operating parameters for both the signal generator and oscilloscope, enabling precise control of measurement conditions. The signal from the generator is sent to an amplifier based on the OPA549 integrated circuit, which is powered by a symmetric voltage from a laboratory power supply to ensure stable operation. The amplifier increases the amplitude of the voltage signal, which is critical for further analysis and processing.

After amplification, the voltage signal is directed to a damper system containing magnetorheological (MR) fluid. The MR fluid changes its properties in the presence of a magnetic field, allowing for controlled damping in the system. A clamp meter monitors the current flowing to the damper, and this meter, connected to the oscilloscope, enables precise current measurements, which are crucial for analyzing the system's dynamic properties. The oscilloscope displays the voltage and current data in real-time and transmits them to the computer for accurate data acquisition and analysis. As a result, the entire measurement system provides high precision and accuracy, essential for advanced research and experimentation.

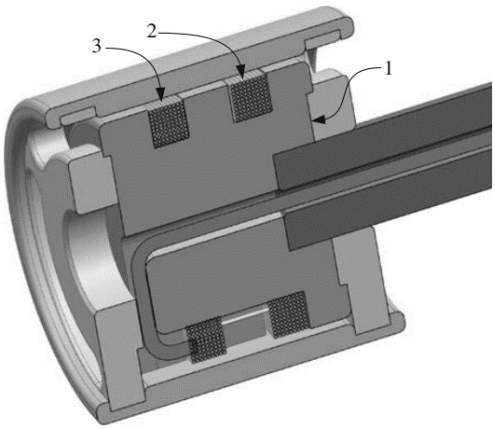

(a) A section of dual-coil piston for MR damper assembly, *1*- core, *2 and 3*- coils [27]

Figure 3. Testing diagram presents all components in the testing loop

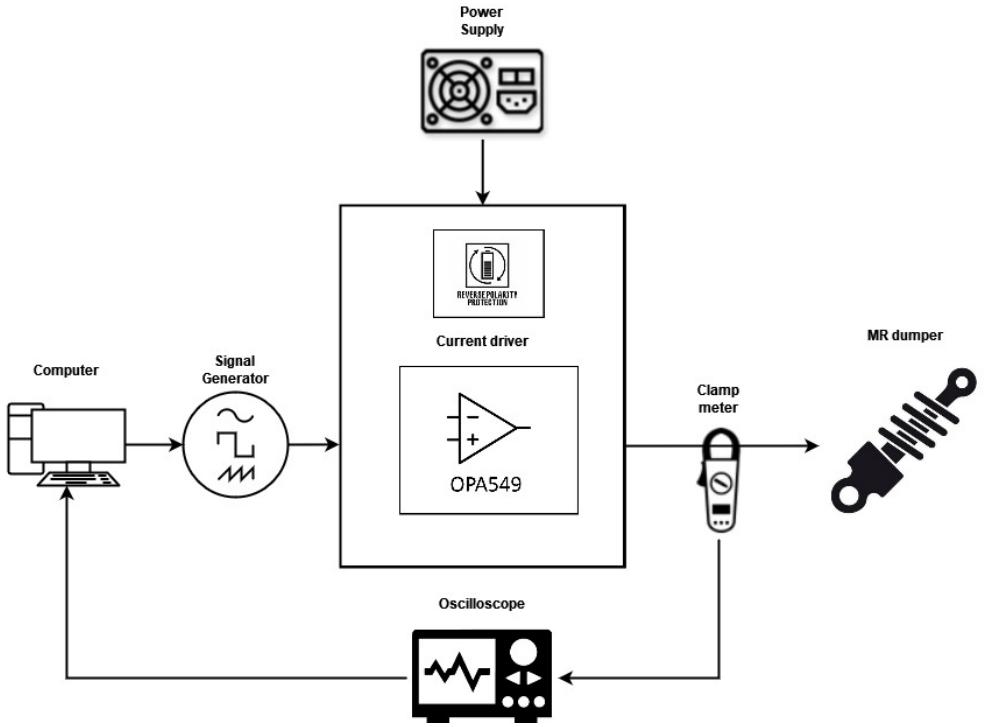

(b) The electrical circuit involving signal generators

Figure 3. (cont.)

However, in these experimental measurements, there was no set compensation for sourcing voltage, so it will be easier to get affected by inductance due to the various encouraging voltage frequencies. It's not necessary to tune up the voltage per frequency if the purpose is just for parameter estimation, where the parameters are regardless of the changing frequency of input voltages as well as output currents. The objective is to investigate flux hysteresis loop effects in greater depth and to conduct further observations.

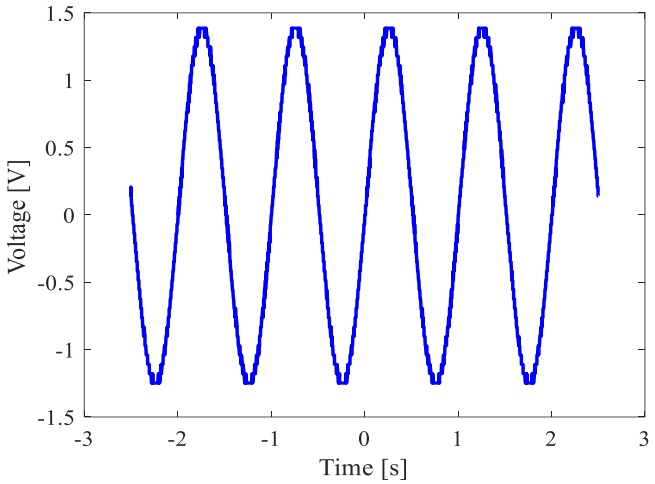

Figure 4. Input voltage for obtaining output signal 1A at frequency 1 Hz

As the input voltage signal was a generated sinusoidal wave, for example, a voltage specified to produce a 1A coil current at 1 Hz, as shown in Figure 4, the desired flux can either be estimated or measured. Figures 5(a), 6(a), and 7(a) compare the experimental results with the model-identified results for flux linkage over time at 1A, 3A, and 5A, respectively. The experimental data appears noisy, with numerous overlaps, particularly evident in Figures 6(b) and 7(b). The direct output coil current and the indirect output flux linkage are mapped from Figure 5(b) to Figure 7(b) to ascertain their relationships, indicating magnetic hysteresis. By analyzing the data from Figures 5-7, the flux model accurately fits the predicted curves to the experimental curves, with strong alignment, especially in cases where the coil current is low.

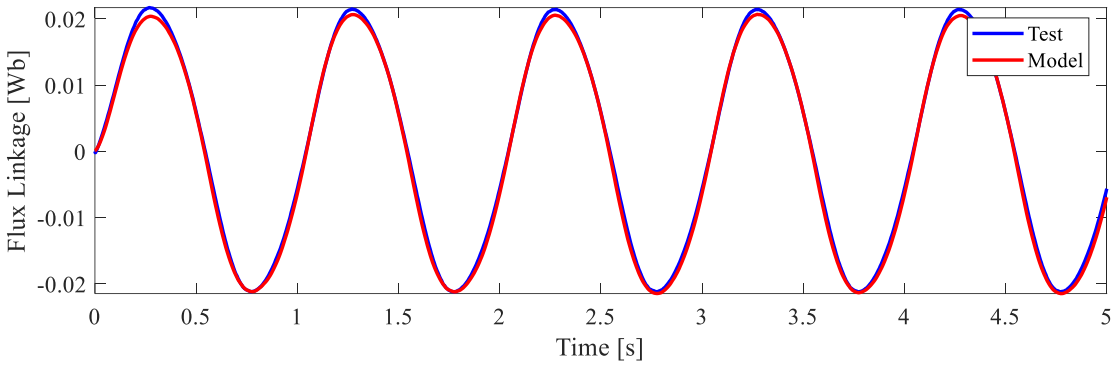

(a) Flux comparison over time between test and model

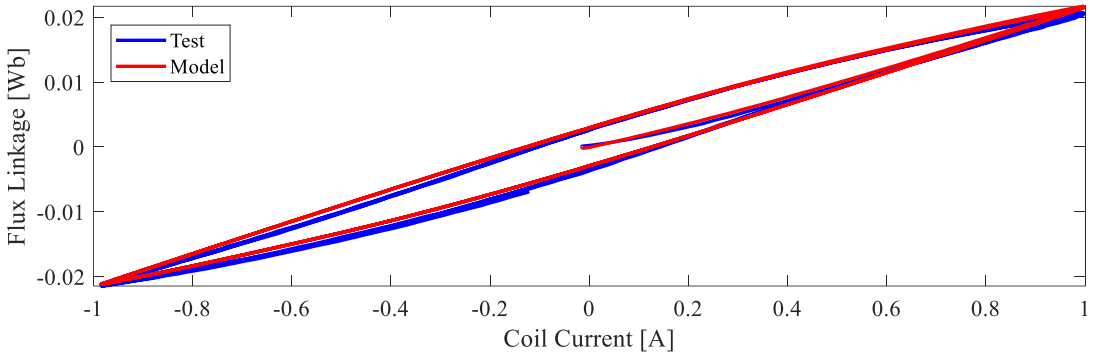

(b) Flux vs current between test and model

Figure 5. Test data comparing with modeling results, I_c = 1A, f = 1Hz

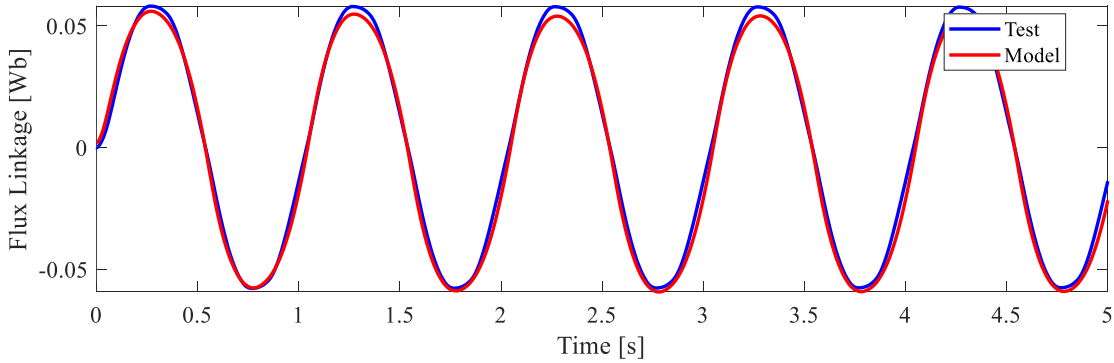

(a) Flux comparison over time between test and model

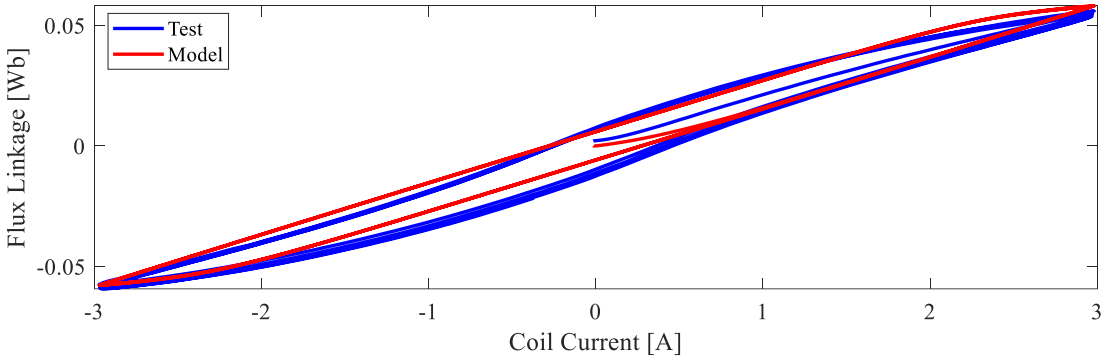

(b) Flux vs current between test and model

Figure 6. Test data comparing with modeling results, I_c = 3A, f = 1Hz

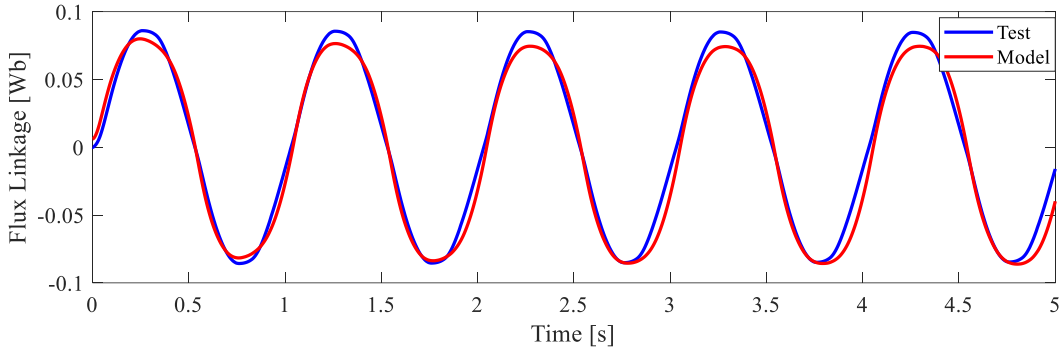

(a) Flux comparison over time between test and model

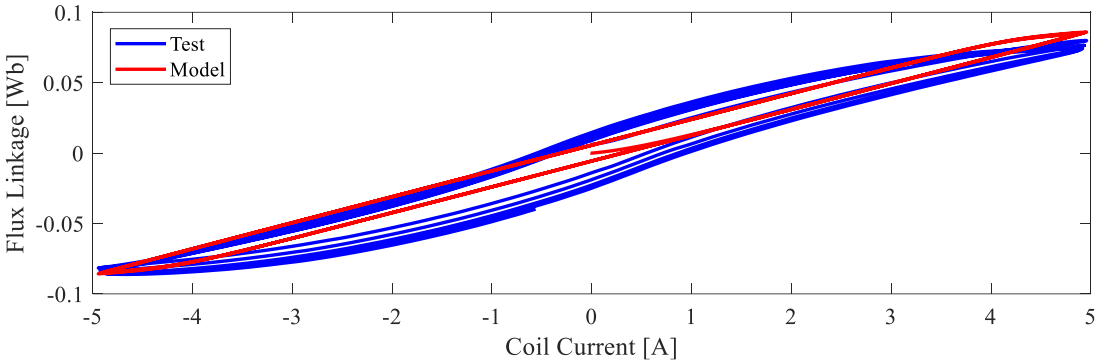

(b) Flux vs current between test and model

Figure 7. Test data comparing with modeling results, I_c = 5A, f = 1Hz

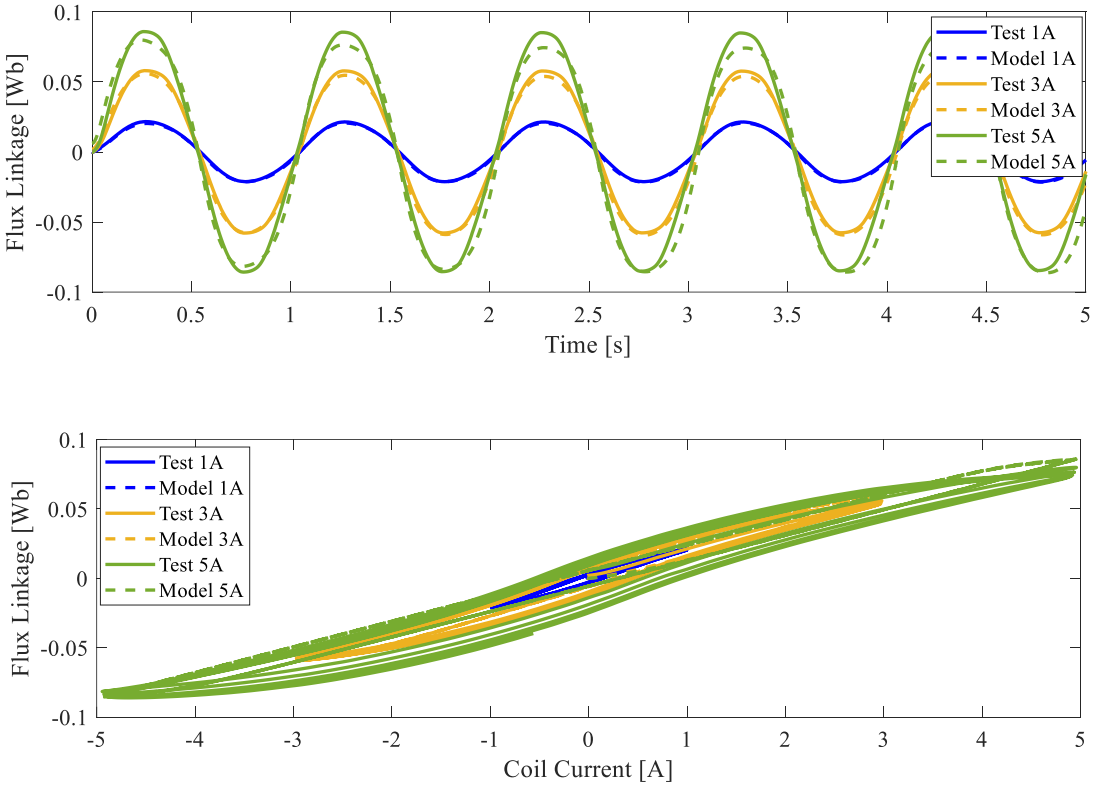

Figure 8. Test data comparing with modeling results, I_c = 1A,3A,5A, f = 1Hz

Figure 8 depicts a map that illustrates the integration of both modeling and experimental data with target currents 1A, 3A, and 5A. The map indicates a positive correlation between the target coil current and magnetic flux. As the current increases, the flux tends to increase as well. Moreover, an increase in the target current results in not only an expansion of the flux-current loop area but also greater visibility of the loop due to the broader current range. It can be observed that a similar trending loop for mechanical hysteresis is present. However, it should be noted that the aforementioned

characteristics can only be identified as either a current-displacement-force or a current-velocity-force relationship if the reconstructed flux model is not formulated. It is important to capture that the operation of magnetic hysteresis demonstrates superior performance at lower currents as well as some medium currents. The device incorporates a hysteresis feature that compares three distinct frequencies: 1 Hz, 5 Hz, and 10 Hz. As illustrated in Figure 9, the width of the flux-current loop exhibits a discernible upward trend as the frequency increases. However, as the input voltage was not compensated for different frequencies, the inductance affected the output coil current. Consequently, a higher frequency has a higher inductance, resulting in a coil current that is not aligned with the target amplitude. This discrepancy will be compensated for in future works by adjusting the voltage.

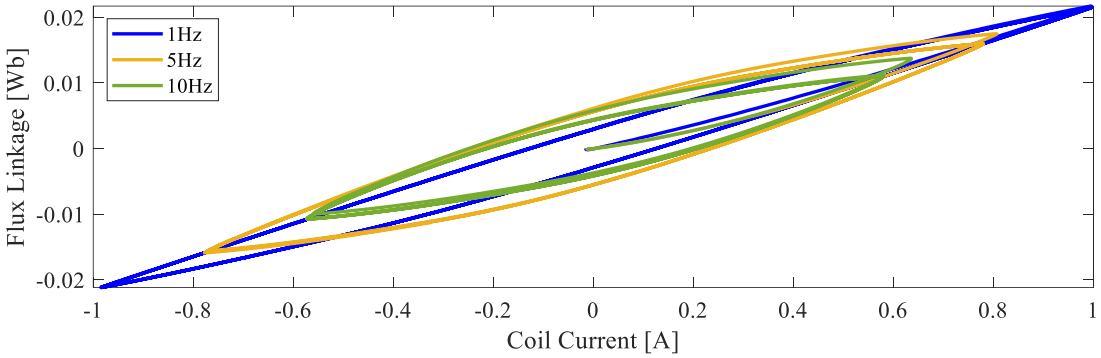

Figure 9. Results comparing in various frequencies, f = 1Hz, 5Hz, 10Hz

In the current study, magnetic hysteresis for the flux model is analyzed without considering frequency effects. Despite this, the experimental data sufficiently validates the feasibility of the flux model and the accuracy of parameter identification. The parameters are clearly defined for the target current, although they show varying degrees of accuracy across different frequencies. Table 1 provides a summary of the standard deviation of estimation results using the PSO-fmincon algorithm. It is observed that lower currents exhibit lower error rates at the same frequency. However, higher frequencies tend to yield more accurate results when comparing the same current across different frequencies.

Table 3 presents the estimated parameters for a 1 Hz signal, Table 4 for a 5 Hz signal, and Table 5 for a 10 Hz signal. Additionally, the authors estimated parameters using the fmincon algorithm, with the results shown in Table 6. To further validate the effectiveness of the proposed PSO-fmincon strategy, Table 2 compares the improvements in standard deviation between the PSO-fmincon and fmincon methods, based on both experimental and simulation results. The proposed algorithm shows an average improvement of 0.38% compared to fmincon results.

The values across different frequencies appear to be highly similar. However, some measurement noise remains, causing slight offsets that need to be addressed. The parameters primarily depend on coil current and vary significantly for different dampers, particularly for different coil types. A visual comparison with the single-coil damper in [28] [29] reveals a notably different range of parameter variations.

Table 1. Standard deviation for different currents per frequency

Current	1Hz	5Hz	10Hz
1A	0.0219	0.0160	0.0121
2A	0.0435	0.0323	0.0270
3A	0.0608	0.0438	0.0371
4A	0.0758	0.0577	0.0450
5A	0.0892	0.0868	0.0657

Table 2. The comparison of standard deviation between PSO-fmincon and fmincon(at 1Hz)

Current	PSO-fmincon	Fmincon	Improvement	Average
1A	0.0219	0.0220	0.46%	
2A	0.0435	0.0436	0.23%	
3A	0.0608	0.0611	0.69%	0.38%
4A	0.0758	0.0761	0.40%	
5A	0.0892	0.0893	0.11%	

Table 3. Estimated parameters, PSO-fmincon (1A to 5A, 1Hz)

Current	A	Lc	κ	β	γ	n	D
1A	1.0957	0.0230	3.4913	29.9979	60.0024	1.3066	20.0008
2A	1.1583	0.0201	3.5300	30.0082	60.0078	1.3014	20.0054
3A	1.1993	0.0178	3.4887	30.0007	59.9993	1.2695	19.9999
4A	1.1990	0.0164	3.4998	29.9999	60.0000	1.3041	20.0000
5A	1.1987	0.0153	3.4990	30.0000	59.9999	1.3041	19.9996

Table 4. Estimated parameters, PSO-fmincon (1A to 5A, 5Hz)

Current	A	k	κ	β	γ	n	D
1A	1.2003	0.0257	3.4993	29.9999	59.9999	1.3001	19.9998
2A	1.1999	0.019	3.4978	29.9993	59.9996	1.2854	19.9988
3A	1.2140	0.0183	3.5473	30.0119	60.0101	1.4805	19.9877
4A	1.1983	0.0162	3.4701	29.9972	59.9995	1.2870	19.9942
5A	1.2244	0.0141	3.5957	29.9764	59.9917	1.2163	20.0003

Table 5. Estimated parameters, PSO-fmincon (1A to 5A, 10Hz)

Current	A	k	κ	β	γ	n	D
1A	1.2156	0.0292	3.505	30.059	59.9545	1.3586	19.6982
2A	1.2008	0.0204	3.4669	29.9968	59.9993	1.2954	19.9952
3A	1.2000	0.0178	3.4879	29.9951	59.9932	1.2506	19.9961
4A	1.1984	0.0161	3.5378	29.9995	60.0013	1.3332	20.0053
5A	1.1909	0.0155	4.2675	29.9446	60.0003	1.8186	19.9146

Table 6. Estimated parameters (fmincon, 1Hz)

Current	A	k	κ	β	γ	n	D
1A	1.1596	0.0220	3.4748	29.997	60.0013	1.2051	19.9949
2A	1.1965	0.0197	3.5105	30.0007	60.0000	1.3000	19.9991
3A	1.1992	0.0180	3.4913	30.0008	59.9995	1.2761	20.0002
4A	1.3016	0.0154	3.5214	30.0014	59.9938	1.3214	19.9806
5A	1.1990	0.0152	3.4989	29.9999	59.9999	1.3005	19.9997

6. CONCLUSIONS

The above-mentioned results demonstrate that magnetic flux hysteresis is a key hysteretic characteristic in magnetorheological dampers, influencing their overall hysteretic behavior. The authors' approach to reconstructing magnetic behavior from the conventional Bouc-Wen model successfully extracts hysteretic properties from force-related hysteresis. The magnetic flux model has been effectively implemented for parameter identification, accurately predicting the model's flux linkage with coil current. This approach allows for addressing magnetic hysteresis to achieve more precise control, either by mitigating its effects or focusing on them. The proposed PSO-fmincon algorithm shows improvements in the standard deviation of 0.46%, 0.23%, 0.69%, 0.40%, and 0.11% for current levels ranging from 1A to 5A, respectively, with an average improvement of 0.38% at a frequency of 1Hz. These improvements were compared with experimental data and modeling results. In all parameter identification cases, experimental data is crucial for accurate predictions. However, the identification process is significantly impacted by the parameters of the magnetic flux model, which exhibit limited variation. Future work should address the need for compensating experimental data for variable frequencies. With the successful validation of the flux model, it is now feasible to implement it for damper control in vehicles. The flux command can drive the desired force more accurately than the current command, which suffers from hysteresis and cannot generate a consistent force response. Further research should continue in this area, as the flux model promises a more precise control mechanism, potentially leading to improved suspension performance.

REFERENCES

[1] I. Bahiuddin, N.A.A. Wahab, M..I Shapiai, S.A. Mazlan, N. Mohamad, F. Imaduddin et al., "Prediction of field-dependent rheological properties of magnetorheological grease using extreme learning machine method," *Journal of Intelligent Material Systems and Structures*, vol. 30, no. 11, pp. 1727-1742, 2019.

[2] J.D Dent, T.E. Lang, "A biviscous modified Bingham model of snow avalanche motion," *Annals of Glaciology*, vol. 4, pp. 42-46, 1983.

[3] S.J. Dyke, B.F. Spencer Jr, M.K. Sain and J.D. Carlson. "Modeling and control of magnetorheological dampers for seismic response reduction," *Smart Materials and Structures*, vol. 5, no. 5, p. 565, 1996.

[4] B.F. Spencer Jr, S.J. Dyke, M.K. Sain and J.D. Carlson, "Phenomenological model for magnetorheological dampers," *Journal of Engineering Mechanics*, vol. 123, no. 3, pp. 230-238, 1997.

[5] G. Yang, B.F. Spencer Jr, H.J. Jung and J.D. Carlson, "Dynamic modeling of large-scale magnetorheological damper systems for civil engineering applications," *Journal of Engineering Mechanics*, vol. 130, no. 9, pp. 107-114, 2004.

[6] S.B. Choi, S.K. Lee and Y.P. Park, "A hysteresis model for the field-dependent damping force of a magnetorheological damper," *Journal of Sound and Vibration*, vol. 2, no. 245, pp. 375-383, 2001.

[7] V. Warke, S.. Kumar, A Bongale, P. Kamat, K. Kotecha, G. Selvachandran et al., "Improving the useful life of tools using active vibration control through data-driven approaches: A systematic literature review," *Engineering Applications of Artificial Intelligence*, vol. 128, p. 107367, 2024.

[8] E.R. Wang, X.Q. Ma, S. Rakheja and C.Y. Su, "Modeling asymmetric hysteretic properties of an mr fluids damper," In *2004 43rd IEEE Conference on Decision and Control (CDC)(IEEE Cat. No. 04CH37601)*, vol. 5, pp. 4643-4648, 2004.

[9] D.M.D. da Silva, S.M. Avila, M.V.G. de Morais and A.A. Cavallini Jr, "Comparing optimization algorithms for parameter identification of sigmoid model for MR damper," *Journal of the Brazilian Society of Mechanical Sciences and Engineering*, vol. 46, no. 3, p. 134, 2024.

[10] I.D. Mayergoyz, G. Friedman and C. Salling "Comparison of the classical and generalized Preisach hysteresis models with experiments," *IEEE Transactions on Magnetics*, vol. 25, no. 5, pp. 3925-3927, 1989.

[11] M.S. Seong, S.B. Choi and Y.M. Han, "Damping force control of a vehicle MR damper using a Preisach hysteretic compensator," *Smart Materials and Structures*, vol. 18, no. 7, p. 074008, 2009.

[12] D.C. Jiles and D.L. Atherton, "Theory of ferromagnetic hysteresis," *Journal of Magnetism and Magnetic Materials*, vol. 61, no. 1-2, pp. 48-60, 1986.

[13] L. Chua and K. Stromsmoe, "Lumped-circuit models for nonlinear inductors exhibiting hysteresis loops," *IEEE Transactions on Circuit Theory*, vol. 17, no. 4, pp. 564-574, 1970.

[14] J.W. Macki, P. Nistri and P. Zecca, "Mathematical models for hysteresis," *SIAM Review*, vol. 35, no. 1, pp. 94-123, 1993.

[15] J. Gołdasz, B. Sapiński, Ł. Jastrzębski and M. Kubik, "Dual hysteresis model of MR dampers," *Frontiers in Materials*, vol. 7, p. 236, 2020.

[16] J. Gołdasz and M. Kubik, "Hysteresis modeling in MR dampers," In *2021 22nd International Carpathian Control Conference (ICCC)*, pp. 1-6, 2021.

[17] X.X. Bai, F.L. Cai and P. Chen, "Resistor-capacitor (RC) operator-based hysteresis model for magnetorheological (MR) dampers," *Mechanical Systems and Signal Processing*, vol. 117, pp. 157-169, 2019.

[18] C.X. Li, "Precise real-time hysteretic force tracking of magnetorheological damper," *Smart Materials and Structures*, vol. 29, no. 10, p. 104002, 2020.

[19] Q.D. Bui, Q.H. Nguyen, X.X.F. Bai and D.D. Mai "A new hysteresis model for magneto–rheological dampers based on Magic Formula," *Proceedings of the Institution of Mechanical Engineers, Part C: Journal of Mechanical Engineering Science*, vol. 235, no. 13, pp. 2437-2451, 2021.

[20] Q.D. Bui, X.X. Bai and Q.H. Nguyen, "Dynamic modeling of MR dampers based on quasi–static model and Magic Formula hysteresis multiplier," *Engineering Structures*, vol. 245, p. 112855, 2021.

[21] A. Kumar, D.K. Gupta, S.R. Ghatak and S.R. Prusty, "A comparison of PSO, GA and FA-based PID controller for load frequency control of two-area hybrid power system," In *Smart Technologies for Power and Green Energy: Proceedings of STPGE 2022*, Singapore: Springer Nature Singapore, pp. 281-292, 2022.

[22] F. Marini and B. Walczak, "Particle swarm optimization (PSO): A tutorial," *Chemometrics and Intelligent Laboratory Systems*, vol. 149, pp. 153-65, 2015.

[23] L. Tang, N.L. Ren and S. Funkhouser, "Semi-active suspension control with PSO tuned LQR controller based on MR damper," *International Journal of Automotive and Mechanical Engineering*, vol. 20, no. 2, pp. 10512-10522, 2023.

[24] M.A. Razman, G. Priyandoko and A.R. Yusoff, "Bouc-Wen model parameter identification for a MR fluid damper using particle swarm optimization," In *Advanced Materials Research*, vol. 903, pp. 279-284, 2014.

[25] Y.Q. Guo, M. Li, Y. Yang, Z.D. Xu and W.H. Xie, "A particle-swarm-optimization-algorithm-improved Jiles–Atherton model for magnetorheological dampers considering magnetic hysteresis characteristics," *Information*, vol. 15, no. 2, p. 101, 2024.

[26] M. Jain, V. Saihjpal, N. Singh and S.B. Singh, "An overview of variants and advancements of PSO algorithm," *Applied Sciences*, vol. 12, no. 17, p. 8392, 2022.

[27] J. Gołdasz, B. Sapiński, J. Gołdasz and B. Sapiński, "Configurations of MR dampers," *Insight into magnetorheological shock absorbers*, pp. 25-49, 2015.

[28] J. Goldasz, B. Sapinski and L. Jastrzebski, "On the application of Bouc-Wen hysteresis approach for modeling of MR actuators," In *ACTUATOR 2018; 16th International Conference on New Actuators*, pp. 1-5, 2018.

[29] M. Kubík and J. Goldasz, "Multiphysics model of an MR damper including magnetic hysteresis," *Shock and Vibration*, vol. 2019, no. 1, p. 3246915, 2019.